HHS Public Access

Author manuscript

Clin Cancer Res. Author manuscript; available in PMC 2020 April 01.

Published in final edited form as:

Clin Cancer Res. 2019 April 01; 25(7): 2278–2289. doi:10.1158/1078-0432.CCR-18-2728.

Broad spectrum activity of the checkpoint kinase 1 inhibitor prexasertib as a single agent or chemopotentiator across a range of preclinical pediatric tumor models

Caitlin D. Lowery[1], **Michele Dowless**[1], **Matthew Renschler**[1], **Wayne Blosser**[1], **Alle B. VanWye**[1], **Jennifer R. Stephens**[1], **Philip W. Iversen**[1], **Aimee Bence Lin**[1], **Richard P. Beckmann**[1], **Kateryna Krytska**[2], **Kristina A. Cole**[2], **John M. Maris**[2], **Douglas S. Hawkins**[3], **Brian P. Rubin**[4], **Raushan T. Kurmasheva**[5], **Peter J. Houghton**[5], **Richard Gorlick**[6], **E. Anders Kolb**[7], **Min H. Kang**[8], **C. Patrick Reynolds**[8], **Stephen W. Erickson**[9], **Beverly A. Teicher**[10], **Malcolm A. Smith**[10], and **Louis F. Stancato**[1]

[1]Eli Lilly and Company, Lilly Corporate Center, Indianapolis, Indiana. [2]The Children's Hospital of Philadelphia, Philadelphia, Pennsylvania. [3]Division of Hematology/Oncology, Seattle Children's Hospital, Seattle, Washington. [4]Departments of Pathology and Cancer Biology, Robert J Tomsich Pathology and Laboratory Medicine Institute and Cleveland Clinic, Cleveland, Ohio. [5]Greehey Children's Cancer Research Institute, San Antonio, Texas. [6]MD Anderson Cancer Center, Houston, Texas. [7]Nemours Center for Cancer and Blood Disorders, Wilmington, Delaware. [8]Texas Tech University Health Sciences Center, Lubbock, Texas. [9]RTI International, Research Triangle Park, North Carolina. [10]National Cancer Institute, Bethesda, Maryland.

Abstract

Purpose: Checkpoint kinase 1 (CHK1) inhibitors potentiate the DNA damaging effects of cytotoxic therapies and/or promote elevated levels of replication stress, leading to tumor cell death. Prexasertib (LY2606368) is a CHK1 small molecule inhibitor under clinical evaluation in multiple adult and pediatric cancers. In this study, prexasertib was tested in a large panel of preclinical models of pediatric solid malignancies alone or in combination with chemotherapy.

Experimental Design: DNA damage and changes in cell signaling following *in vitro* prexasertib treatment in pediatric sarcoma cell lines were analyzed by western blot and high content imaging. Anti-tumor activity of prexasertib as a single agent or in combination with different chemotherapies was explored in cell line-derived (CDX) and patient-derived xenograft (PDX) mouse models representing nine different pediatric cancer histologies.

Results: Pediatric sarcoma cell lines were highly sensitive to prexasertib treatment *in vitro*, resulting in activation of the DNA damage response. Two PDX models of desmoplastic small round cell tumor and one malignant rhabdoid tumor CDX model responded to prexasertib with complete regression. Prexasertib monotherapy also elicited robust responses in mouse models of

Corresponding Author: Louis F. Stancato, Oncology Translational Research, Lilly Corporate Center, Indianapolis, Indiana 46285, Phone: 317-655-6910, Fax: 317-276-1414, stancato_louis@lilly.com.

Conflict of Interest Statement: Caitlin D. Lowery, Michele Dowless, Matthew Renschler, Wayne Blosser, Alle B. VanWye, Jennifer Stephens, Philip Iversen, Aimee Bence Lin, and Richard Beckmann are full-time employees of Eli Lilly and Company.

rhabdomyosarcoma. Concurrent administration with chemotherapy was sufficient to overcome innate resistance or prevent acquired resistance to prexasertib in preclinical models of neuroblastoma, osteosarcoma, and Ewing's sarcoma, or alveolar rhabdomyosarcoma, respectively.

Conclusion: Prexasertib has significant anti-tumor effects as a monotherapy or in combination with chemotherapy in multiple preclinical models of pediatric cancer. These findings support further investigation of prexasertib in pediatric malignancies.

Keywords

Prexasertib; CHK1; checkpoint kinase 1; pediatric cancer

Introduction

Cancer is the leading cause of death from disease in children and adolescents, with approximately 20% of patients dying within 5 years of diagnosis (1). Despite substantial research which has uncovered molecular mechanisms driving the development and progression of pediatric cancers, standard of care generally consists of systemic cytotoxic chemotherapy, radiation, and/or surgery and prognosis of patients with recurrent, refractory, or advanced disease remains poor (2–4). In addition, these aggressive multimodal regimens often result in debilitating chronic and/or late treatment effects and even secondary cancers for pediatric cancer survivors (5). It is therefore essential to identify and evaluate novel targeted therapies across pediatric cancer types to improve patient outcome and potentially limit treatment-associated conditions.

Checkpoint kinase 1 (CHK1) is a serine/threonine kinase with critical roles in the DNA damage response and the regulation of replication initiation (6). Full activation of CHK1 following DNA damage (single-strand breaks) or replication fork stalling (leading to long stretches of exposed single-strand DNA) requires phosphorylation at serines 317 and 345 by ataxia telangiectasia and Rad3-related protein (ATR) and autophosphorylation at serine 296 (7). Activated CHK1 promotes an S or G2/M phase cell cycle arrest through downregulation of the CDC25A and CDC25C phosphatases, which are responsible for removing inhibitory phosphates on cyclin-dependent kinase 1 and 2 (CDK1 and CDK2) and thus facilitate cell cycle progression. Loss of CHK1 through genetic manipulation or pharmacologic inhibition results in abrogation of the S and G2/M cell cycle checkpoints and diminished DNA damage response, leading to double-strand DNA breaks, increased replication stress (RS), and cancer cell death due to replication catastrophe (6,8–10).

Inhibitors of CHK1 have historically been used to potentiate the DNA damaging effects of chemotherapy or radiation (6); however, recent clinical and non-clinical studies have demonstrated single agent activity of newer CHK1 inhibitors in both adult and pediatric cancers (6,8,10–14). Prexasertib (LY2606368) is a small molecule inhibitor of CHK1 shown previously to reduce cell viability at nanomolar concentrations across a panel of well-characterized human cancer cell lines representing a wide range of adult and pediatric malignancies (10,15). A focused evaluation in preclinical models of adult cancers revealed that prexasertib caused extensive DNA damage leading to cell death via replication catastrophe (8). Furthermore, preclinical models of neuroblastoma, a relatively common

pediatric tumor, were found to be highly sensitive to prexasertib monotherapy (10). In this study, we expand upon our previous findings in neuroblastoma and demonstrate broad prexasertib activity, either as monotherapy or in combination with chemotherapy, across a wide array of preclinical pediatric cancer models.

Methods

Cell culture conditions

Human pediatric sarcoma cell lines A673 (Ewing's sarcoma, cat#CRL-1598), MG-63 (osteosarcoma, cat#CRL-1427), SJCRH30 (alveolar rhabdomyosarcoma [aRMS], cat# CRL-2061), and RD (embryonal RMS [eRMS], cat#CCL-136) were purchased from American Type Culture Collection (ATCC). The alveolar RMS cell line Rh41 was obtained from St. Jude's Children Research Hospital (Memphis, TN). Cells were grown in the media recommended by the respective vendor or institution and tested negative for Mycoplasma prior to freezing down working stocks. Additional cell lines were generated and maintained by the Pediatric Preclinical Testing Consortium (PPTC) (16). Cell lines were authenticated by STR-based DNA profiling and multiplex PCR. Cells were maintained at 37°C and 5% CO_2 in tissue-culture treated flasks.

Test compound

Preclinical studies use LY2940930, which is the mesylate monohydrate salt of LY2606368 (prexasertib, Eli Lilly and Company), and will be referred to as prexasertib for the purposes of this study. Prexasertib was dissolved in DMSO to a stock concentration of 10 mM for *in vitro* use and prepared in 20% Captisol™ for *in vivo* experiments.

Cell proliferation assay

Evaluation of cell proliferation 72h post-treatment with prexasertib over a range of concentrations (starting at 1 μM with 3-fold dilutions) was performed using the CellTiter Glo™ Luminescent Cell Viability Assay (Promega, cat#G7571). For each cell line, luminescence was normalized to the average of the DMSO-treated control. Analysis of cell proliferation following 96h of prexasertib treatment was conducted as previously described using digital image fluorescence microscopy to quantify live cells (16). Relative EC_{50} values were calculated from triplicate experiments using GraphPad Prism 7 (GraphPad Software, Inc., Version 7.00). An estimate of the relationship between of input cell number (0h) and the number of cells at 96h (In/Out%) was made based on the doubling time of each cell line using the 96h fluorescence values for the control and treated lines. In/Out% values range between −100% (complete cytotoxicity) to +100% (no treatment effect), with 0% indicating no change in cell number between 0h and 96h.

Western blot analysis

Cell lysis, SDS-PAGE, and immunoblotting were performed as previously described (10). Cells or tumor pieces were lysed in 1% SDS (Fisher BioReagents, cat#BP2436–200) supplemented with 1x HALT protease and phosphatase inhibitor (ThermoFisher, cat#78441). The following antibodies were purchased from Cell Signaling: CHK1 (cat#2360), CHK1 S296 (cat#90178), CHK1 S345 (cat#234), WEE1 (cat#4936), WEE1

S642 (cat#4910), PARP (cat#9542), AKT (cat#9272), AKT S473 (cat#4060), ERK1/2 (cat#4695), ERK1/2 T202/Y204 (cat#4370), MEK1/2 (cat#4694), MEK1/2 S217/221 (cat#9154), and BCL-xL (cat#2764). Additional antibodies included CHK2 (StressGen, cat#KAM-CC112), RPA32/2 (AbCam, cat#ab61184), RPA32/2 S4/8 (Bethyl, cat#A300–245), γH2AX (Millipore, cat#05–636), and GAPDH (Millipore, cat#MAB374).

Immunofluorescence

High content cell imaging and subsequent analysis were conducted as previously described (10,17,18). Antibodies were as follows: γH2AX (Millipore, cat#05–636), cleaved caspase 3 (Cell Signaling, cat#9661), ATM S1981 (Millipore, cat# 05–740), and DNA-PKcs S2056 (AbCam, cat#ab18192). AlexaFluor secondary antibodies were purchased from ThermoFisher. All antibodies were used at a 1:200 dilution. DNA was stained with Hoescht 33342 diluted 1:5000. Cells were imaged using a CellInsight NXT platform and analyzed by the TargetActivation V.4 Bioapplication (Thermo Scientific). Percent responders (percent positive for desired marker) were gated based on the DMSO-treated group for each cell line.

In vivo evaluation of prexasertib

In vivo studies were performed in accordance with American Association for Laboratory Animal Care institutional guidelines. Cell line-derived xenograft (CDX) *in vivo* experiments were approved by the Eli Lilly and Company Animal Care and Use Committee. *In vivo* experiments utilizing patient-derived xenograft (PDX) models designated by codes starting with ‘CTG’ were conducted at Champions Oncology (Hackensack, NJ). PDX models with names starting with ‘ST’ were conducted at START (San Antonio, TX). The CCSARC005 osteosarcoma PDX model was generated through a collaboration with the Cleveland Clinic and evaluated at Covance, Inc (Indianapolis, IN). For *in vivo* studies run by the PPTC, full methodology is available in the Supplementary Methods.

To evaluate prexasertib on CDX growth, cells were harvested during log phase growth and resuspended in Hank’s Balanced Salt Solution (HBSS). Suspended cells were diluted 1:1 with BD Matrigel Matrix (cat#356234; only used for Rh41 and RD-ES) and 5×10^6 cells (A673, Rh41, or SJCRH30) or 10×10^6 cells (RD-ES) were injected subcutaneously into the right flank of female CB-17 SCID beige mice. When tumor volumes averaged ~200 mm^3, mice were randomized into treatment groups. Animals were given vehicle (20% Captisol™ in water, pH 4), prexasertib, chemotherapy (doxorubicin, cisplatin, cyclophosphamide, irinotecan, or irinotecan + temozolomide [TMZ]), or a combination of prexasertib and chemotherapy. Combination partners were dependent on the tumor model. Prexasertib (10 mg/kg) was administered by subcutaneous injection twice daily for 3 days followed by 4 days rest (BIDx3D, restx4D) for 3 or 4 weeks. Chemotherapy was given as follows: doxorubicin, 5 mg/kg once weekly (Q7D; iv); cisplatin, 4 mg/kg once weekly (Q7D; ip); cyclophosphamide, 100 mg/kg once weekly (Q7D; ip); irinotecan, 2.5 mg/kg daily for 5 days, rest for 14 days (QDx5, rest 14D; ip); TMZ, 66mg/kg, once daily for 5 days then rested for 16 days (QDx5, restx16; po) for as many weeks as prexasertib was administered. Prexasertib was given at a reduced dose of 8 mg/kg (BIDx3D, restx4D) when co-administered with the following small molecule inhibitors: pan-RAF inhibitor (LY3074753; 25 mg/kg BIDx21, po), ERK inhibitor (LY3214996; 50 mg/kg BIDx21, po), or PI3K/mTOR

inhibitor (LY3023414; 7.5 mg/kg BIDx21, po). Modifications in dose or schedule are mentioned in the summary table and/or figure legend where appropriate. All combinations were considered tolerable, as body weight loss did not exceed 10% (data not shown).

Tumor volume was transformed to a log scale to equalize variance across time and treatment groups. Log volume data was analyzed with a two-way repeated measures analysis of variance by time and treatment using the MIXED procedures in SAS software (Version 9.3). The correlation model for the repeated measures was Spatial Power. Treated groups were compared to the control group at each time point. The MIXED procedure was also used separately for each treatment group to calculate adjusted means and standard errors at each time point. The BLISS independence method was used to define a statistically significant effect in combination studies. Combinations were defined as additive if the combination arm was statistically different from both of the single agent arms. Procedures for *in vivo* testing by the PPTC are as described by Houghton *et al* (19). Additional details for PPTC *in vivo* data analysis are provided in the Supplementary Methods.

Results

Pediatric cancer cell lines are highly sensitive to prexasertib in vitro

The broad antiproliferative activity of prexasertib was demonstrated previously across a range of adult and pediatric tumor types at clinically achievable concentrations, while proliferation of normal cell types (melanocytes and endothelial colony forming cells) was largely unaffected (10). Consistent with these findings, prexasertib potently reduced proliferation in 25 pediatric cancer cell lines corresponding to 12 different histologies at low nanomolar concentrations (relative EC_{50} range: 0.9 – 22 nM; Table 1, Supplementary Fig. S1). Response was not influenced by histology or p53 status and most cell lines showed evidence of cytotoxicity according to the median In/Out% value (that is, the relationship between the cell number at time 0 [In] to that at 96h post-prexasertib treatment [Out]) (16) of −91% (Supplementary Table S1). However, RD, BT-12, and CHLA-266 cells had positive In/Out% values between 0 and 25%, indicating limited effects of prexasertib treatment in these cell lines.

Five pediatric cancer cell lines representing different childhood sarcomas – A673 (Ewing's sarcoma); MG-63 (osteosarcoma); RD (embryonal rhabdomyosarcoma [eRMS]); and Rh41 and SJCRH30 (alveolar RMS [aRMS]) – were analyzed for changes in cell signaling following *in vitro* treatment with prexasertib. Reduction in CHK1 autophosphorylation at S296 indicated that kinase activity was diminished following 24h of treatment in all cell lines evaluated (Fig. 1A). Interestingly, WEE1, a downstream effector of CHK1 and a key modulator of the G2-M checkpoint following DNA damage, was readily detected by immunoblot in SJCRH30 and Rh41 but not in the other 3 cell lines evaluated; decreased phosphorylation of WEE1 in both aRMS cell lines further demonstrated prexasertib-mediated CHK1 inhibition (Fig. 1A). Furthermore, CDK1, CDK2, and CDC25A/C protein levels were relatively unchanged following prexasertib treatment in all cell lines evaluated with the exception of SJCRH30, in which an increase in both CDK2 and CDC25A total protein was noted (Supplementary Fig. S2).

Elevated total and phosphorylated replication protein A 32/2 (RPA32/2) protein levels pointed to an increase in exposed single-strand DNA following CHK1 inhibition (Fig. 1A). The appearance of γH2AX-immunopositive nuclei of treated cells was noted as early as 2h post-treatment and was markedly increased after 24h, indicating the accumulation of double-strand DNA breaks (Fig. 1B *left*, Supplementary Fig. S3A *bottom*, Supplementary Table S2). Prexasertib also led to the activation of DNA damage response machinery responsible for double-strand break repair as measured by phosphorylation of CHK1 at S345 and of DNA damage sensors ataxia telangiectasia mutated (ATM) and DNA protein kinase (DNA-PK) at serine 1981 (S1981) and serine 2056 (S2056), respectively (Fig. 1A and B *right*, Supplementary Table S2). In contrast to previous observations in neuroblastoma cell lines (10), cleaved caspase 3 following prexasertib treatment was low in all five cell lines (approximately 20% of cells with 1 μM prexasertib; Fig. 1B *left*, Supplementary Table S2) and a strong cleaved PARP signal was only detected in Rh41 and SJCRH30 aRMS cell lines (Fig. 1A). However, a marked reduction in both nuclei count and DNA synthesis (as marked by EdU positivity) and a dose-dependent increase in cell death (as evidenced by TUNEL staining) were observed at 24 and 48 hours post-treatment in 4 of the 5 cell lines evaluated (A673 being the exception; Supplementary Fig. S3).

Prexasertib has significant single agent activity in pediatric NB, DSRCT, and RMS xenografts

Prexasertib monotherapy was tested across 38 cell line-derived (CDX) and patient-derived xenograft (PDX) mouse models corresponding to 9 different pediatric solid tumor types (Fig. 2). Clinically relevant plasma concentrations for prexasertib monotherapy were achieved using a dosing schedule of 10 mg/kg prexasertib twice daily for 3 days followed by 4 days of rest for 3–4 cycles (8,20). As observed previously (10), neuroblastoma PDX models were sensitive to prexasertib, with 50% of the models responding with stable disease (COG-N-421x, NB-1643x, and NB-SDx) and the other three models demonstrating partial regression (COG-N-453x, COG-N-Felix-x, and NB-EBc1-x) (Fig. 2). In addition, prexasertib was highly active in several soft tissue tumor models, many of which were refractory to doxorubicin or other standard of care chemotherapy (Fig. 3, Supplementary Table S3). Interestingly, prexasertib induced tumor regression in two PDX models of desmoplastic small round cell tumor (DSRCT) (Fig. 3A and B, Supplementary Tables S3 and S4, Supplementary Fig. S4A and B). While durable responses were achieved in CTG-1458 following prexasertib monotherapy, tumor regrowth was observed in CTG-0926 approximately 2 months post-treatment. Re-treatment with prexasertib resulted in durable tumor regression indicating the xenografts remained sensitive to therapy (Fig. 3B). Similarly, two aRMS models (SJCRH30 CDX and ST162 PDX) responded to single agent prexasertib with rapid tumor regression (Fig. 3C and D, Supplementary Table S3, Supplementary Fig. S4C and D). However, unlike the retained prexasertib sensitivity observed in the CTG-0926 DSRCT model, re-emergent aRMS tumors appeared to develop acquired resistance to prexasertib. Indeed, SJCRH30 tumors continued to grow during the rechallenge with prexasertib and ST162 xenografts only responded with tumor stasis while on treatment. Post-treatment western blot analysis of SJCRH30 xenografts revealed elevated levels of the anti-apoptotic protein BCL-xL in tumors which acquired resistance when compared to vehicle-treated tumors (Supplementary Fig. S5A); furthermore, activated PI3K and MAPK

signaling was also detected in resistant tumors as measured by increased phosphorylation of AKT, MEK1/2, and ERK1/2. However, prexasertib co-treatment with an inhibitor of RAF (LY3074753), ERK (LY3214996), or PI3K/mTOR (LY3023414) did not prevent the emergence of resistance to prexasertib in the SJCRH30 model (Supplementary Fig. S5B).

Additional pediatric soft tissue tumor models responded to single agent prexasertib during treatment, and their behavior post-treatment was highly model-dependent. Stable disease was achieved in two eRMS PDX models, CTG-1213 and CTG-1116, with a durable response observed in CTG-1213 (Fig. 3E and F, Supplementary Table S3, Supplementary Fig. S4E and F). Furthermore, different responses to prexasertib were observed in MRT *in vivo* models (Fig. 2, Supplementary Table S3) with complete regression of RBD-1 xenografts, stable disease in KT-12 and KT-13, and progressive disease observed in the A-204 model. Interestingly, evaluation of prexasertib in 'n of 1' studies across 11 PDX models of leiomyosarcoma and liposarcoma, the most common adult STS subtypes, revealed that the majority of these PDXs responded with delayed tumor growth (albeit still progressive disease); furthermore, two leiomyosarcoma models achieved stable disease (Supplementary Fig. S6). Taken together, these data suggest that soft tissue histologies generally exhibit sensitivity to prexasertib preclinically, though the overall response is highly variable and likely model dependent.

Most Ewing's sarcoma and osteosarcoma preclinical models are resistant to prexasertib monotherapy

There was a trend of pediatric soft tissue and neuroblastoma tumor models being more sensitive to prexasertib than models of pediatric tumors involving bone (i.e. Ewing's sarcoma and osteosarcoma) (Fig. 2). Only one of 14 Ewing's sarcoma xenograft models responded to single agent prexasertib (Fig. 4A, Supplementary Tables S3–S5, Supplementary Fig. S4G); of the 7 osteosarcoma models tested, stable disease was only achieved with prexasertib monotherapy in the CTG-0242 model (Fig. 4B, Supplementary Table S3, Supplementary Fig. S4H). The remaining Ewing's sarcoma and osteosarcoma xenograft models progressed during treatment with prexasertib or chemotherapy as single agents (Fig. 4C–F, Supplementary Tables S3–S6, Supplementary Fig. S4I–L and S7) with the exception of partial regressions achieved with single agent cyclophosphamide in the RD-ES CDX model (Fig. 4F, Supplementary Fig. S4L), suggesting that the majority of Ewing's sarcoma and osteosarcoma models tested may be intrinsically resistant to prexasertib and DNA-damaging drugs as single agents.

Combination with chemotherapy abrogates acquired resistance to prexasertib and promotes durable responses in pediatric tumor models

As CHK1 inhibitors are often used as chemopotentiators, prexasertib was also evaluated in combination with chemotherapies that are typically administered as pediatric cancer therapy. Mice bearing SJCRH30 aRMS xenografts were treated with prexasertib, doxorubicin, cyclophosphamide, irinotecan, or the combination of prexasertib plus each agent. Consistent with prior experiments, SJCRH30 tumors initially regressed and acquired resistance occurred towards the end of prexasertib monotherapy (Fig. 5A and B), while a slight tumor growth delay was observed with each of the individual chemotherapies. While tumor

regrowth was observed in animals given prexasertib alone, combination of prexasertib plus individual cytotoxics was strongly additive and regressions were maintained in all animals (Fig. 5A and B, Supplementary Table S4, Supplementary Fig. S4M). Similarly, combination of prexasertib with chemotherapy was superior to monotherapy in Rh41 aRMS xenografts and prevented tumor regrowth following cessation of treatment (Fig. 5C, Supplementary Table S4, Supplementary Fig. S4N). Previously, our group reported that mouse models of neuroblastoma initially regressed in response to prexasertib; however, tumor regrowth was observed post-treatment in 2 models and was not prevented by combination with doxorubicin (10). To better understand whether this response is model-dependent, prexasertib was evaluated in combination with irinotecan in 2 additional neuroblastoma models (Supplementary Table S4, Supplementary Fig. S8). While prexasertib or irinotecan alone significantly impaired NB-Felix-x tumor growth, this effect was more pronounced when the two agents were combined (Supplementary Fig. S8A). In addition, prexasertib plus irinotecan resulted in complete regression of NB-EBc1-x xenografts and no regrowth was observed following the cessation of treatment (Supplementary Fig. S8B). When prexasertib was tested at a lower dose (4 mg/kg twice daily, days 1, 3, 5) in combination with irinotecan, significant prolongation in time to event was observed for only 1 out of 6 neuroblastoma xenografts and 1 of 2 rhabdoid tumor models but no combination effect was noted for the alveolar rhabdomyosarcoma models evaluated (Supplementary Table S6).

Prexasertib plus chemotherapy yields additive anti-tumor effects in osteosarcoma and Ewing’s sarcoma tumor models

Combination treatment was assessed in osteosarcoma and Ewing’s sarcoma tumor models that displayed intrinsic resistance to prexasertib (including models responding with delayed but progressive tumor growth). Treatment with prexasertib or cisplatin alone had a minor effect on CCSARC005 osteosarcoma xenograft growth when compared to the vehicle-treated arm; however, the combination was greater than additive and resulted in stable disease (Fig. 5D, Supplementary Table S4, Supplementary Fig. S4O). In the A673 Ewing’s sarcoma CDX model, tumor growth delay was observed with prexasertib or irinotecan monotherapy. Again, combination effects were greater than additive in this model, with 40% of the animals achieving stable disease and 60% partial regression (Fig. 5E, Supplementary Table S4, Supplementary Fig. S4P). When prexasertib was tested at a lower dose (4 mg/kg twice daily, days 1, 3, 5) in combination with irinotecan, significant prolongation in time to event was observed for 2 osteosarcoma xenografts, but not for the evaluated Ewing’s sarcoma model (Supplementary Figure S7, Supplementary Table S6).

For combination studies, dosing of prexasertib and chemotherapy were given concurrently and began on day 1 of each cycle (Fig. 5, Supplementary Tables S4 and S5, Supplementary Fig. S7 and S8). However, sequential administration of each agent could potentially improve response to therapy through the generation and/or exacerbation of DNA damage and inhibition of repair. To test whether a DNA-damaging agent plus prexasertib would give a superior anti-tumor response if dosing was staggered, mice bearing A673 Ewing’s sarcoma CDXs were treated with cyclophosphamide and prexasertib concurrently, with cyclophosphamide on day 1 (D1) and prexasertib on D2–4 of each cycle, or with prexasertib on D1–3 and cyclophosphamide on D4 of each cycle (Supplementary Fig. S9 *left*).

Interestingly, concurrent treatment resulted in a significant tumor regression while the best response achieved in either staggered therapy arm was stable disease. Additional study arms evaluating the combination of prexasertib and the microtubule-destabilizer vincristine determined that there was no difference in response between concurrent or staggered administration of these drugs (Supplementary Fig. S9 *right*).

Discussion

In response to DNA damage or disruptions to DNA replication, including stalled replication forks or difficult-to-navigate secondary structures, CHK1 promotes S or G2/M phase cell cycle arrest, stabilizes stalled forks, and inhibits late replication origin firing, thus mitigating replication stress (RS) and promoting cell survival (21). Loss of CHK1 function can lead to cell death via replication catastrophe due to uncontrolled replication origin firing and depletion of the nucleotide pool, persistent DNA damage via increased double-strand DNA breaks, loss of DNA damage checkpoints, and a delayed or inhibited DNA damage response (6). Pharmacologic inhibition of CHK1 has historically been used as a tool to potentiate the DNA-damaging effects of chemotherapy or radiation (6). Recently, single agent CHK1 inhibitor activity has been reported in preclinical cancer models (8,10,13,14) and in phase I and II clinical trials (11,20,22), indicating that in some tumor types CHK1 is critical for cell survival beyond its integral role in the DNA damage response. In this study, we report that prexasertib (LY2606368), a second-generation CHK1 inhibitor, is active as a monotherapy or in combination with chemotherapy across a range of preclinical pediatric cancer models.

Consistent with data generated using a large panel of cancer cell lines (10,15), prexasertib was universally anti-proliferative at clinically relevant concentrations for monotherapy across 25 pediatric cancer cell lines representing 12 different histologies; however, *in vivo* evaluation revealed differential model-dependent responses to prexasertib. In addition to the previously reported neuroblastoma sensitivity (10), most soft tissue sarcoma (STS) *in vivo* models evaluated in this study (including two DSRCT PDXs and several RMS models) were sensitive to prexasertib monotherapy while both Ewing's and osteosarcoma models were generally resistant, suggesting that STS subtypes may rely more heavily on CHK1 for cancer progression than bony tumors. However, as the majority of adult leiomyosarcoma and liposarcoma models tested continued to grow despite prexasertib-mediated CHK1 inhibition, it is clear that not all STS models exhibit sensitivity to monotherapy and that histology alone is insufficient to predict both the type and degree of *in vivo* response to prexasertib.

RS, a cellular state of dysregulated DNA replication due to oncogene activation, genomic instability, and persistent DNA damage (21), is as a potential indicator of sensitivity to CHK1 blockade. CHK1 inhibition exacerbates RS by allowing increased and/or unscheduled replication origin firing as well as a delay or loss of DNA repair. Though most pediatric cancers have a lower mutational burden (and therefore fewer targets available for therapeutic intervention) than adult malignancies (23), known drivers of some childhood tumors, such as chimeric transcription factors (24), can trigger RS (25) and may promote tumor cell sensitivity to CHK1 inhibition. At first glance, using fusion protein expression as a surrogate for an elevated state of RS in order to predict response to prexasertib monotherapy is supported by our extensive *in vivo* data. DSRCT, a malignancy of adolescence and young

adulthood that carries a 5-year survival rate of only 15%, and for which therapeutic options are extremely limited (26), is characterized by the *EWS-WT1* fusion protein. Both DSRCT PDX models responded to prexasertib with tumor regression; furthermore, sensitivity was retained in CTG-0926 tumors that regrew following initial prexasertib treatment. Robust partial regressions occurred in aRMS models expressing the PAX3-FOXO1 fusion protein, while fusion-negative models of eRMS only achieved stable disease. However, the ability to exclusively link the expression of any oncogenic fusion protein to prexasertib activity was thwarted by the intrinsic resistance to prexasertib displayed by the majority of *EWS-FLI* fusion-positive Ewing's sarcoma mouse models, though the possibility remains that the degree of chimeric transcription factor-driven RS depends on additional histology-dependent aberrations, i.e. not all fusion proteins drive RS equally.

Oncogene-induced RS (such as that caused by overexpression and/or amplification of *MYC* proteins) can force tumor cells to rely more heavily on the ATR/CHK1 axis for suppression of RS (27,28) and allow for a synthetic lethal approach to selectively target this cell population with prexasertib. *MYCN* amplification, observed in approximately 20% of neuroblastoma (and 50% of high-risk cases), is associated with poor patient prognosis (29); in addition, *MYCN*-amplified/high-risk primary tumors expressed higher levels of CHK1 mRNA than non-*MYCN*-amplified/low-risk tumors (9). siRNA-mediated CHK1 knockdown was cytotoxic in a panel of neuroblastoma cell lines (9) and preclinical neuroblastoma mouse models were highly sensitive to single agent prexasertib (10); however, these results were not dependent on *MYCN* status. Similarly, while many of the prexasertib-sensitive neuroblastoma models evaluated in this study harbored *MYCN* amplification (NB-SDx, COG-NB-453x, COG-NB-421x) (30), stable disease and partial regressions were achieved in mice bearing non-*MYCN*-amplified neuroblastoma (NB-Felix-x and NB-EBc1-x); moreover, NB-1643x was the least responsive model despite the presence of the *MYCN* amplicon. Therefore, it is likely that an additional RS-promoting genetic insult is necessary for an anti-tumor response to prexasertib monotherapy in neuroblastoma and other highly sensitive pediatric cancer models.

Acquired prexasertib resistance observed in two aRMS mouse models following the initial dosing period may have resulted from either a new mutation or other novel alterations which rendered tumor cells resistant to subsequent CHK1 inhibition, or the selection of a pre-existing resistant population. The relatively short time to tumor regrowth combined with the activation of pro-survival PI3K/mTOR and MAPK signaling pathways in resistant tumors, as well as the observation that upfront combination with cytotoxic chemotherapy prevents acquired resistance (presumably through elimination of intrinsically prexasertib-resistant tumor cells), supports the latter hypothesis. Increased ERK1/2 phosphorylation in response to CHK1 inhibition has been reported in several cancer cell lines (31–34); furthermore, concurrent administration of the CHK1 inhibitor AZD7762 and selumetinib (AZD6244, a MEK1/2 inhibitor) *in vitro* promoted apoptosis in multiple myeloma cells, but not normal bone marrow cells (31). However, upfront combination of a MAPK or PI3K/mTOR pathway inhibitor with prexasertib was insufficient to prevent SJCRH30 xenograft regrowth in this study, potentially reflective of the low baseline signaling in treatment-naïve tumors; therefore, targeted inhibition of RAF, ERK, or PI3K/mTOR may have better anti-tumor

activity in re-emergent tumors that reacted to prexasertib with activated pro-survival signaling.

Combining prexasertib with chemotherapy commonly used in the pediatric cancer setting produced superior anti-tumor effects in models of Ewing's sarcoma and osteosarcoma and increased response durability in neuroblastoma and aRMS xenografts, demonstrating its chemopotentiation capability. The reduced chemopotentiation at a lower prexasertib dose highlights the importance of optimizing prexasertib dose when it is used in combinations. Other studies have demonstrated that CHK1 inhibitors sensitize pediatric tumor cells and xenograft models (including Ewing's sarcoma and neuroblastoma) to gemcitabine, a ribonucleotide reductase inhibitor (35,36). Another preclinical study described the synergistic interaction between prexasertib and the purine nucleoside antimetabolite clofarabine in pediatric acute lymphocytic leukemia (ALL) cell lines or the multi-tyrosine kinase inhibitors imatinib and dasatinib in adult ALL cells (37). These data indicate that prexasertib can not only be effectively combined with traditional cytotoxics, but also with targeted inhibitors to elicit superior anti-tumor activity. In addition, co-targeting CHK1 and its downstream effector WEE1 in cell lines and xenografts from genetically engineered mouse models of neuroblastoma resulted in increased double-strand DNA breaks and cell death through mitotic catastrophe and significant tumor growth delay, respectively (38). Additional studies have also reported synergism between inhibitors of CHK1 and WEE1, ATR, or PARP in preclinical models of different tumor types (14,39–43). Targeting multiple nodes within the same signaling pathway (i.e. a 'vertical blockade') to achieve a greater therapeutic benefit is not without precedent as evidenced by the combination of RAF and MEK inhibitors in metastatic melanoma (44). Taken together, these reports suggest that prexasertib may combine well with cytotoxic drugs currently used in pediatric cancer patient care or with other targeted agents.

Schedule-based administration of prexasertib and chemotherapy may boost the anti-tumor activity of the combination. If chemotherapy is given first, the resultant DNA damage could persist with the subsequent administration of a CHK1 inhibitor. In either case, the possibility remains that RS resulting from significant DNA damage would lead to cell death via replication catastrophe. Treatment with gemcitabine prior to CHK1 inhibition (and thus promoting RS through depletion of the nucleotide pool) resulted in greater anti-tumor activity when compared to concurrent administration in a panel of carcinoma cell lines and xenografts (45–47). Similarly, gemcitabine given approximately 24h prior to administration of the first-generation CHK1 inhibitor LY2603618 promoted superior combination effects in several xenografts of adult carcinomas (48). In contrast, our data support concurrent administration of prexasertib and cyclophosphamide, as greater than additive combination effects were observed with this schedule, but not with either staggered dosing schedule, in mice bearing A673 Ewing's sarcoma xenografts; however, treatment schedules may be influenced by the mechanism of action of the chemotherapy or other agents used in combination with prexasertib and/or by tumor model. Therefore, further preclinical evaluation in additional pediatric models is necessary to optimize dosing schedules when combining prexasertib with different chemotherapies or targeted agents.

While overall survival of pediatric cancer patients has improved dramatically over recent decades, the prognosis of children with certain tumor types, including those with high-risk and relapsed disease, remains poor; moreover, the development of targeted therapies for pediatric indications is limited (49). Identification and evaluation of novel targeted agents is essential to improve prognosis while reducing long-term treatment-associated toxicities, an endeavor complicated by low incidence of pediatric cancer, a wide variety of histological types, and a general paucity of actionable genetic aberrations at initial diagnosis (23,49). As this study demonstrates through our finding of profound single agent activity in mouse models of DSRCT, continued preclinical exploration of prexasertib in childhood cancer may yield new therapeutic indications for this vulnerable patient population. Moreover, two phase II clinical trials are focused on evaluating prexasertib monotherapy in adult tumors that exhibit increased levels of RS or deficiencies in DNA repair (NCT02873975, NCT02203513), demonstrating the potential clinical utility of identifying and validating drivers of RS for pediatric cancers. Recently published clinical studies have focused on identification and evaluation of potential genetic determinants of prexasertib response in adult squamous cell carcinoma and high grade serous ovarian cancer patient samples collected from ongoing phase I and II trials (11,22), and we are compiling genomic characterization data from all preclinical models included in this study to interrogate putative predictive biomarkers of prexasertib response. The results of the ongoing Phase 1 clinical study of prexasertib in pediatric patients (NCT02808650) combined with nonclinical data provide direction for translating our results to clinical evaluation of prexasertib in high-risk pediatric patients with soft tissue tumors.

Supplementary Material

Refer to Web version on PubMed Central for supplementary material.

Acknowledgements

PPTC funding: Gorlick: U01 CA199221; Houghton: U01 CA199297; RTI Coordinating Center (Gatto): U01 CA199287; Maris: U01 CA199222; PPTC funding: Houghton: Contract #HHSN261201000001C. John Maris is the Giulio D'Angio Endowed Chair and NIH grant recipient R35 CA220500.

Financial support: This study was funded by Eli Lilly and Company, Lilly Corporate Center, Indianapolis, Indiana, USA.

Works Cited

1. Jemal A, Ward EM, Johnson CJ, Cronin KA, Ma J, Ryerson B, et al. Annual Report to the Nation on the Status of Cancer, 1975–2014, Featuring Survival. J Natl Cancer Inst 2017;109(9).
2. Adamson PC. Improving the outcome for children with cancer: Development of targeted new agents. CA Cancer J Clin 2015;65(3):212–20. [PubMed: 25754421]
3. Kurmasheva RT, Houghton PJ. Identifying novel therapeutic agents using xenograft models of pediatric cancer. Cancer Chemotherapy and Pharmacology 2016;78(2):221–32. [PubMed: 27193096]
4. Anderson JL, Denny CT, Tap WD, Federman N. Pediatric sarcomas: translating molecular pathogenesis of disease to novel therapeutic possibilities. Pediatr Res 2012;72(2):112–21. [PubMed: 22546864]

5. Bhakta N, Liu Q, Ness KK, Baassiri M, Eissa H, Yeo F, et al. The cumulative burden of surviving childhood cancer: an initial report from the St Jude Lifetime Cohort Study (SJLIFE). Lancet 2017;390(10112):2569–82. [PubMed: 28890157]
6. Lin AB, McNeely SC, Beckmann RP. Achieving Precision Death with Cell-Cycle Inhibitors that Target DNA Replication and Repair. Clin Cancer Res 2017;23(13):3232–40. [PubMed: 28331049]
7. Karnitz LM, Zou L. Molecular Pathways: Targeting ATR in Cancer Therapy. Clinical Cancer Research 2015;21(21):4780–85. [PubMed: 26362996]
8. King C, Diaz HB, McNeely S, Barnard D, Dempsey J, Blosser W, et al. LY2606368 Causes Replication Catastrophe and Antitumor Effects through CHK1-Dependent Mechanisms. Mol Cancer Ther 2015;14(9):2004–13. [PubMed: 26141948]
9. Cole KA, Huggins J, Laquaglia M, Hulderman CE, Russell MR, Bosse K, et al. RNAi screen of the protein kinome identifies checkpoint kinase 1 (CHK1) as a therapeutic target in neuroblastoma. Proc Natl Acad Sci U S A 2011;108(8):3336–41. [PubMed: 21289283]
10. Lowery CD, VanWye AB, Dowless M, Blosser W, Falcon BL, Stewart J, et al. The Checkpoint Kinase 1 Inhibitor Prexasertib Induces Regression of Preclinical Models of Human Neuroblastoma. Clin Cancer Res 2017;23(15):4354–63. [PubMed: 28270495]
11. Lee JM, Nair J, Zimmer A, Lipkowitz S, Annunziata CM, Merino MJ, et al. Prexasertib, a cell cycle checkpoint kinase 1 and 2 inhibitor, in BRCA wild-type recurrent high-grade serous ovarian cancer: a first-in-class proof-of-concept phase 2 study. Lancet Oncol 2018;19(2):207–15. [PubMed: 29361470]
12. Bryant C, Rawlinson R, Massey AJ. Chk1 inhibition as a novel therapeutic strategy for treating triple-negative breast and ovarian cancers. BMC Cancer 2014;14:570. [PubMed: 25104095]
13. Sakurikar N, Thompson R, Montano R, Eastman A. A subset of cancer cell lines is acutely sensitive to the Chk1 inhibitor MK-8776 as monotherapy due to CDK2 activation in S phase. Oncotarget 2016;7(2):1380–94. [PubMed: 26595527]
14. Sen T, Tong P, Stewart CA, Cristea S, Valliani A, Shames DS, et al. CHK1 Inhibition in Small-Cell Lung Cancer Produces Single-Agent Activity in Biomarker-Defined Disease Subsets and Combination Activity with Cisplatin or Olaparib. Cancer Res 2017;77(14):3870–84. [PubMed: 28490518]
15. May CD, Beckmann R, Blosser W, Dowless M, VanWye A, Burke T, et al. Targeting checkpoint kinase 1 (CHK1) with the small molecule inhibitor LY2606368 mesylate monohydrate in models of high-risk pediatric cancer yields significant antitumor effects. AACR; 2016.
16. Kang MH, Smith MA, Morton CL, Keshelava N, Houghton PJ, Reynolds CP. National Cancer Institute pediatric preclinical testing program: model description for in vitro cytotoxicity testing. Pediatr Blood Cancer 2011;56(2):239–49. [PubMed: 20922763]
17. Low J, Huang S, Blosser W, Dowless M, Burch J, Neubauer B, et al. High-content imaging characterization of cell cycle therapeutics through in vitro and in vivo subpopulation analysis. Mol Cancer Ther 2008;7(8):2455–63. [PubMed: 18723491]
18. Low J, Shuguang H, Dowless M, Blosser W, Vincent T, Davis S, et al. High-content imaging analysis of the knockdown effects of validated siRNAs and antisense oligonucleotides. J Biomol Screen 2007;12(6):775–88. [PubMed: 17517903]
19. Houghton PJ, Morton CL, Tucker C, Payne D, Favours E, Cole C, et al. The pediatric preclinical testing program: description of models and early testing results. Pediatr Blood Cancer 2007;49(7): 928–40. [PubMed: 17066459]
20. Hong D, Infante J, Janku F, Jones S, Nguyen LM, Burris H, et al. Phase I Study of LY2606368, a Checkpoint Kinase 1 Inhibitor, in Patients With Advanced Cancer. J Clin Oncol 2016;34(15): 1764–71. [PubMed: 27044938]
21. Kotsantis P, Petermann E, Boulton SJ. Mechanisms of Oncogene-Induced Replication Stress: Jigsaw Falling into Place. Cancer Discov 2018.
22. Hong DS, Moore KN, Patel MR, Grant SC, Burris HA, William WN, et al. Evaluation of Prexasertib, a Checkpoint Kinase 1 Inhibitor, in a Phase Ib Study of Patients with Squamous Cell Carcinoma. Clin Cancer Res 2018.

23. Grobner SN, Worst BC, Weischenfeldt J, Buchhalter I, Kleinheinz K, Rudneva VA, et al. The landscape of genomic alterations across childhood cancers. Nature 2018;555(7696):321–27. [PubMed: 29489754]
24. Dupain C, Harttrampf AC, Urbinati G, Geoerger B, Massaad-Massade L. Relevance of Fusion Genes in Pediatric Cancers: Toward Precision Medicine. Mol Ther Nucleic Acids 2017;6:315–26. [PubMed: 28325298]
25. Gorthi A, Romero JC, Loranc E, Cao L, Lawrence LA, Goodale E, et al. EWS–FLI1 increases transcription to cause R-loops and block BRCA1 repair in Ewing sarcoma. Nature 2018;555(7696):387. [PubMed: 29513652]
26. Dufresne A, Cassier P, Couraud L, Marec-Berard P, Meeus P, Alberti L, et al. Desmoplastic small round cell tumor: current management and recent findings. Sarcoma 2012;2012:714986. [PubMed: 22550424]
27. Murga M, Campaner S, Lopez-Contreras AJ, Toledo LI, Soria R, Montana MF, et al. Exploiting oncogene-induced replicative stress for the selective killing of Myc-driven tumors. Nat Struct Mol Biol 2011;18(12):1331–35. [PubMed: 22120667]
28. Rohban S, Campaner S. Myc induced replicative stress response: How to cope with it and exploit it. Biochim Biophys Acta 2015;1849(5):517–24. [PubMed: 24735945]
29. Bosse KR, Maris JM. Advances in the translational genomics of neuroblastoma: From improving risk stratification and revealing novel biology to identifying actionable genomic alterations. Cancer 2016;122(1):20–33. [PubMed: 26539795]
30. Harenza JL, Diamond MA, Adams RN, Song MM, Davidson HL, Hart LS, et al. Transcriptomic profiling of 39 commonly-used neuroblastoma cell lines. Sci Data 2017;4:170033. [PubMed: 28350380]
31. Pei XY, Dai Y, Youssefian LE, Chen S, Bodie WW, Takabatake Y, et al. Cytokinetically quiescent (G0/G1) human multiple myeloma cells are susceptible to simultaneous inhibition of Chk1 and MEK1/2. Blood 2011;118(19):5189–200. [PubMed: 21911831]
32. Booth L, Cruickshanks N, Ridder T, Dai Y, Grant S, Dent P. PARP and CHK inhibitors interact to cause DNA damage and cell death in mammary carcinoma cells. Cancer Biol Ther 2013;14(5): 458–65. [PubMed: 23917378]
33. Dent P, Tang Y, Yacoub A, Dai Y, Fisher PB, Grant S. CHK1 inhibitors in combination chemotherapy: thinking beyond the cell cycle. Mol Interv 2011;11(2):133–40. [PubMed: 21540473]
34. Lee HJ, Cao Y, Pham V, Blackwood E, Wilson C, Evangelista M, et al. Ras-MEK Signaling Mediates a Critical Chk1-Dependent DNA Damage Response in Cancer Cells. Mol Cancer Ther 2017;16(4):694–704. [PubMed: 28138032]
35. Xu H, Cheung IY, Wei XX, Tran H, Gao X, Cheung NK. Checkpoint kinase inhibitor synergizes with DNA-damaging agents in G1 checkpoint-defective neuroblastoma. Int J Cancer 2011;129(8): 1953–62. [PubMed: 21154747]
36. Goss KL, Koppenhafer SL, Harmoney KM, Terry WW, Gordon DJ. Inhibition of CHK1 sensitizes Ewing sarcoma cells to the ribonucleotide reductase inhibitor gemcitabine. Oncotarget 2017;8(50): 87016–32. [PubMed: 29152060]
37. Ghelli Luserna Di Rora A, Iacobucci I, Imbrogno E, Papayannidis C, Derenzini E, Ferrari A, et al. Prexasertib, a Chk1/Chk2 inhibitor, increases the effectiveness of conventional therapy in B-/T-cell progenitor acute lymphoblastic leukemia. Oncotarget 2016;7(33):53377–91. [PubMed: 27438145]
38. Russell MR, Levin K, Rader J, Belcastro L, Li Y, Martinez D, et al. Combination therapy targeting the Chk1 and Wee1 kinases shows therapeutic efficacy in neuroblastoma. Cancer Res 2013;73(2): 776–84. [PubMed: 23135916]
39. Magnussen GI, Emilsen E, Giller Fleten K, Engesaeter B, Nahse-Kumpf V, Fjaer R, et al. Combined inhibition of the cell cycle related proteins Wee1 and Chk1/2 induces synergistic anti-cancer effect in melanoma. BMC Cancer 2015;15:462. [PubMed: 26054341]
40. Hauge S, Naucke C, Hasvold G, Joel M, Rodland GE, Juzenas P, et al. Combined inhibition of Wee1 and Chk1 gives synergistic DNA damage in S-phase due to distinct regulation of CDK activity and CDC45 loading. Oncotarget 2017;8(7):10966–79. [PubMed: 28030798]

41. Chaudhuri L, Vincelette ND, Koh BD, Naylor RM, Flatten KS, Peterson KL, et al. CHK1 and WEE1 inhibition combine synergistically to enhance therapeutic efficacy in acute myeloid leukemia ex vivo. Haematologica 2014;99(4):688–96. [PubMed: 24179152]

42. Kim H, George E, Ragland R, Rafial S, Zhang R, Krepler C, et al. Targeting the ATR/CHK1 Axis with PARP Inhibition Results in Tumor Regression in BRCA-Mutant Ovarian Cancer Models. Clin Cancer Res 2017;23(12):3097–108. [PubMed: 27993965]

43. Brill E, Yokoyama T, Nair J, Yu M, Ahn YR, Lee JM. Prexasertib, a cell cycle checkpoint kinases 1 and 2 inhibitor, increases in vitro toxicity of PARP inhibition by preventing Rad51 foci formation in BRCA wild type high-grade serous ovarian cancer. Oncotarget 2017;8(67):111026–40. [PubMed: 29340034]

44. Long GV, Hauschild A, Santinami M, Atkinson V, Mandalà M, Chiarion-Sileni V, et al. Adjuvant Dabrafenib plus Trametinib in Stage III BRAF-Mutated Melanoma. New England Journal of Medicine 2017;377(19):1813–23. [PubMed: 28891408]

45. Montano R, Thompson R, Chung I, Hou H, Khan N, Eastman A. Sensitization of human cancer cells to gemcitabine by the Chk1 inhibitor MK-8776: cell cycle perturbation and impact of administration schedule in vitro and in vivo. BMC Cancer 2013;13:604. [PubMed: 24359526]

46. Blackwood E, Epler J, Yen I, Flagella M, O'Brien T, Evangelista M, et al. Combination drug scheduling defines a "window of opportunity" for chemopotentiation of gemcitabine by an orally bioavailable, selective ChK1 inhibitor, GNE-900. Mol Cancer Ther 2013;12(10):1968–80. [PubMed: 23873850]

47. Montano R, Khan N, Hou H, Seigne J, Ernstoff MS, Lewis LD, et al. Cell cycle perturbation induced by gemcitabine in human tumor cells in cell culture, xenografts and bladder cancer patients: implications for clinical trial designs combining gemcitabine with a Chk1 inhibitor. Oncotarget 2017;8(40):67754–68. [PubMed: 28978069]

48. Barnard D, Diaz HB, Burke T, Donoho G, Beckmann R, Jones B, et al. LY2603618, a selective CHK1 inhibitor, enhances the anti-tumor effect of gemcitabine in xenograft tumor models. Invest New Drugs 2016;34(1):49–60. [PubMed: 26612134]

49. Stewart CF, Robinson GW. Development of Molecularly Targeted Therapies to Treat Pediatric Malignancies. Clin Pharmacol Ther 2017;102(5):752–53. [PubMed: 28836264]

Statement of Translational Relevance

Prexasertib (LY2606368) is a small molecule inhibitor of checkpoint kinase 1 (CHK1) currently in Phase I and II clinical trials as a single agent and in combination with chemotherapy in adult patients with advanced cancers. For pediatric cancer patients, there are limited therapeutic options available and survivors often suffer from debilitating chronic conditions related to intensive therapeutic intervention. In this study, we demonstrate preclinically that prexasertib is active as a single agent in specific subtypes of pediatric sarcoma and neuroblastoma and can also act as a chemopotentiator when combined with cytotoxic chemotherapy. These data further support the ongoing clinical investigation of prexasertib in pediatric patients with recurrent or refractory solid tumors (NCT02808650) and nominates future combinatorial therapeutic strategies.

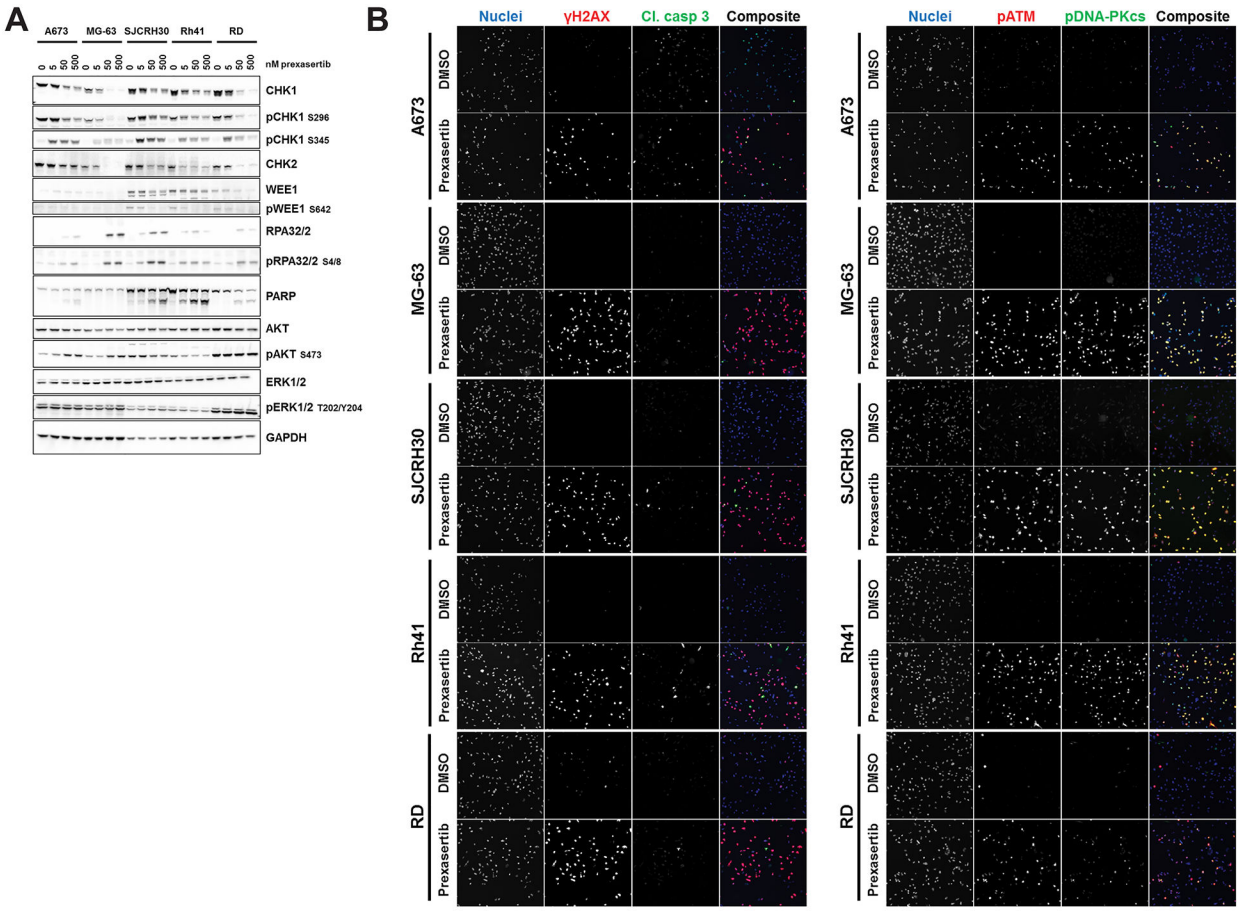

Figure 1. Prexasertib-mediated CHK1 inhibition promotes DNA double-strand breaks resulting in activation of the DNA damage response in vitro.

A, Whole cell lysates of pediatric sarcoma cell lines treated with increasing concentrations of prexasertib over 24h were probed for the indicated total and phosphorylated proteins. **B**, Cells were treated with prexasertib over a range of concentrations for 24h prior to fixation and immunostaining. Representative images show cells treated with DMSO or 111 nM prexasertib and were taken at 20× magnification using the appropriate filters for each channel. Experiments were conducted twice. (*Left*) Red: γH2AX; green: cleaved caspase 3; blue: DNA. (*Right*) Red: ATM phosphorylated at serine 1981; green: DNA-PKcs phosphorylated at serine 2056; blue: DNA.

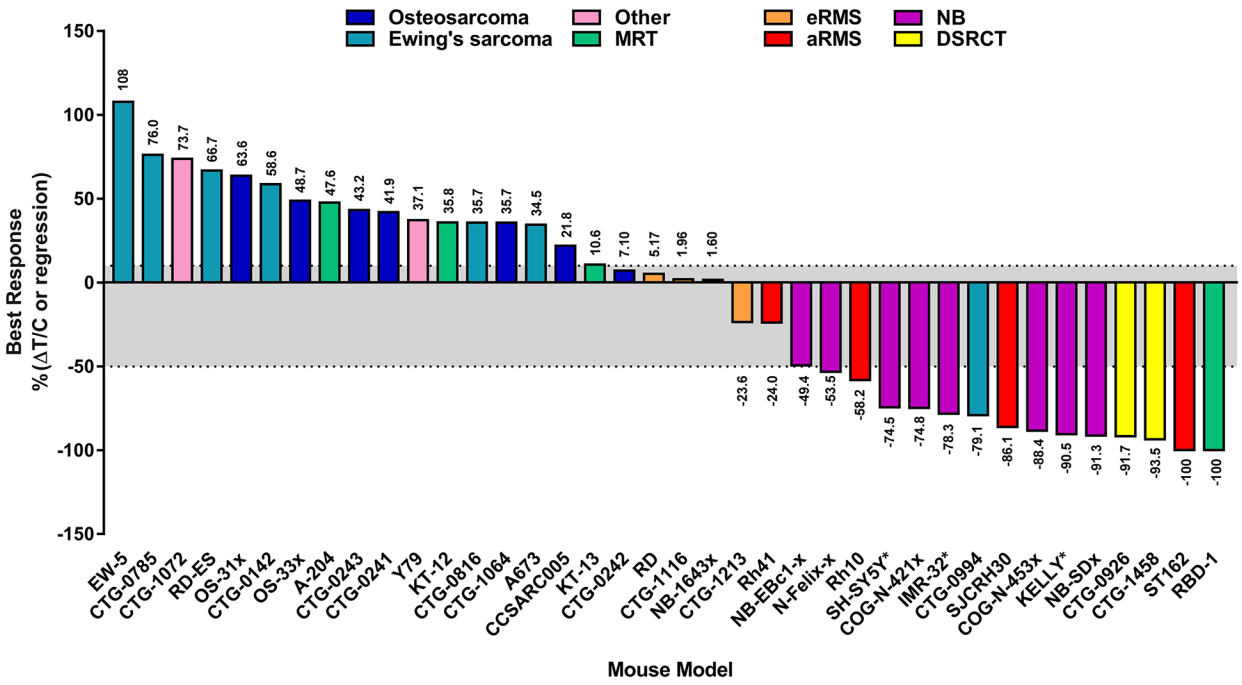

Figure 2. Prexasertib is active as a single agent in preclinical models of pediatric soft tissue tumors.

The best response achieved with prexasertib monotherapy was determined by averaging the responses of individual mice in each model (n ≥ 4 mice/arm) and is indicated above (%ΔT/C) or below (%regression) each bar. Gray shading indicates stable disease. aRMS: alveolar rhabdomyosarcoma; eRMS: embryonal rhabdomyosarcoma; DSRCT: desmoplastic small round cell tumor; MRT: malignant rhabdoid tumor; NB: neuroblastoma; Other: hepatoblastoma (CTG-1072), retinoblastoma (Y79). * denotes neuroblastoma models that were previously published in (10) Lowery CD, et al. Clin Cancer Res 2017;23(15):4354–63.

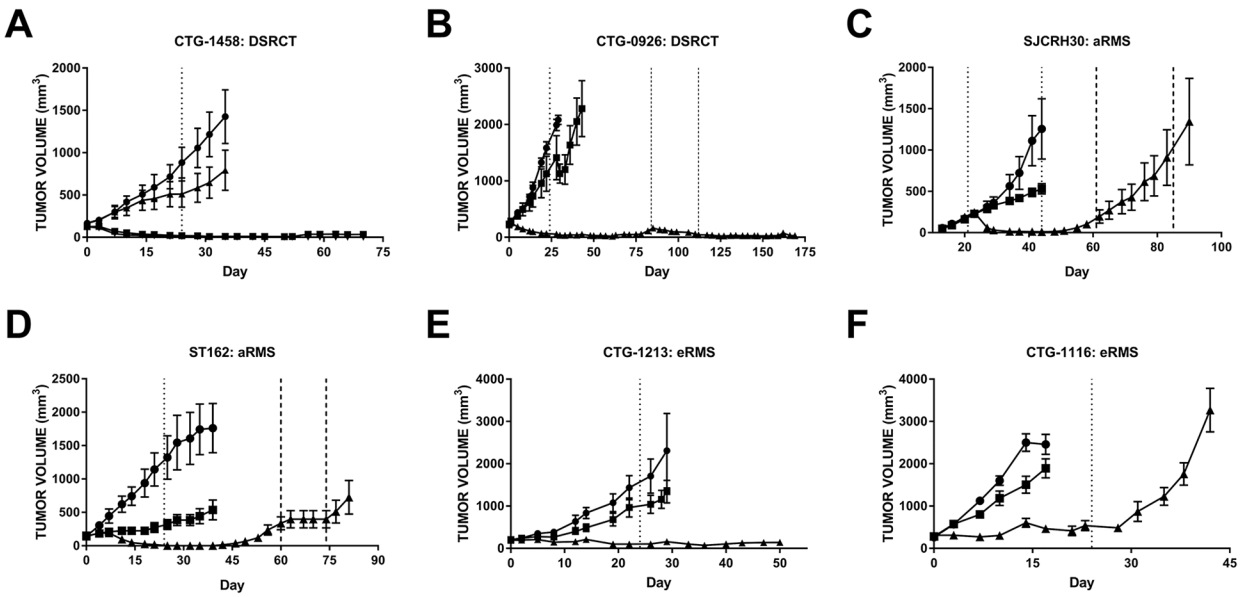

Figure 3. Prexasertib monotherapy elicits superior anti-tumor responses to chemotherapy in pediatric mouse models of soft tissue sarcoma.

All animals were treated with vehicle (●), chemotherapy (■, doxorubicin unless otherwise indicated), or prexasertib (▲). Dosing began at day 0 and treatment end is indicated by dotted lines. Additional treatment periods are indicated by darker dashed lines. **A**, CTG-1458 desmoplastic small round cell tumor (DSRCT) PDX, ■ = cyclophosphamide; ▼ = combination of prexasertib and cyclophosphamide, n = 5/arm. Prexasertib single agent and combination arms overlap for the entirety of the study. **B**, CTG-0926 DSRCT PDX, n = 5/arm. **C**, SJCRH30 alveolar RMS CDX, n = 6/arm. **D**, ST162 alveolar RMS PDX, n = 4/arm. **E**, CTG-1213 embryonal RMS PDX, n = 5/arm, ■ = actinomycin D. **F**, CTG-1116 embryonal RMS PDX, n = 4/arm. Error bars: SEM. Waterfall plots for each model are shown in Supplementary Fig. S4 and statistical analyses are summarized in Supplementary Table S2.

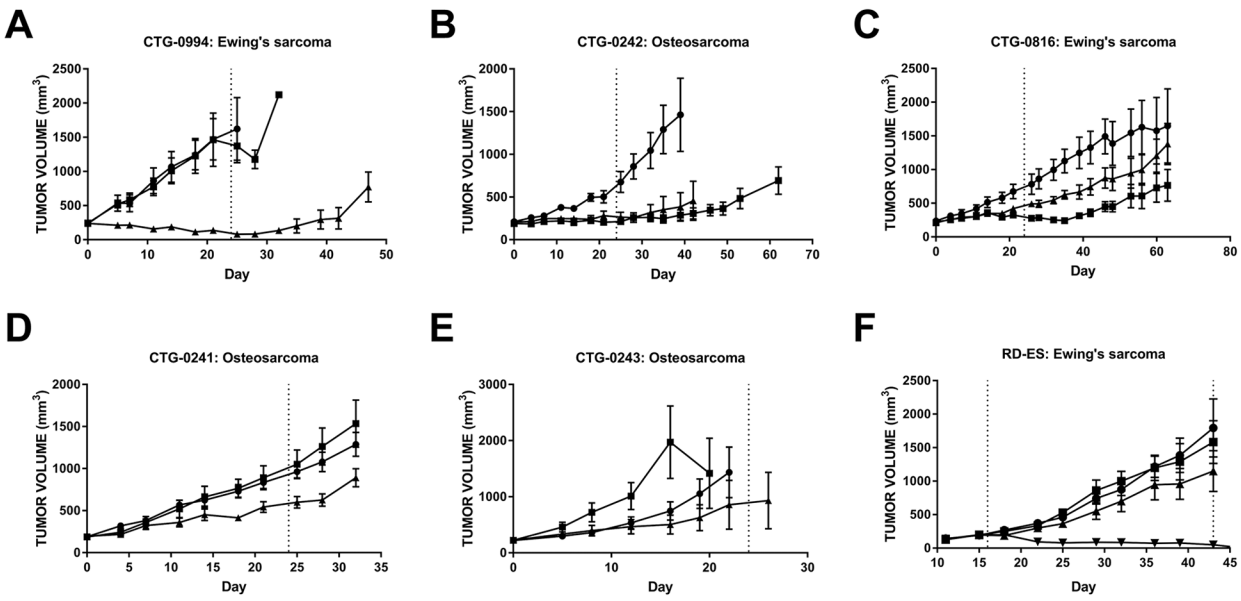

Figure 4. Majority of Ewing's sarcoma and osteosarcoma mouse models exhibit intrinsic resistance to prexasertib.

All animals were treated with vehicle (●), doxorubicin (■), or prexasertib (▲). The dosing interval is bracketed by dotted lines; if treatment began at day 0, the single dotted line marks end of treatment. Additional treatment periods are indicated by darker dashed lines. **A**, CTG-0994 Ewing's sarcoma PDX, n = 5/arm. **B**, CTG-0242 osteosarcoma PDX, n = 5/arm. **C**, CTG-0816 Ewing's sarcoma PDX, n = 5/arm. **D**, CTG-0241 osteosarcoma PDX, n = 5/arm. **E**, CTG-0243 osteosarcoma PDX, n = 5/arm. **F**, RD-ES Ewing's sarcoma CDX, ■ = cyclophosphamide, n = 8/arm. Error bars: SEM. Waterfall plots for each model are shown in Supplementary Fig. S4 and statistical analyses are summarized in Supplementary Table S2.

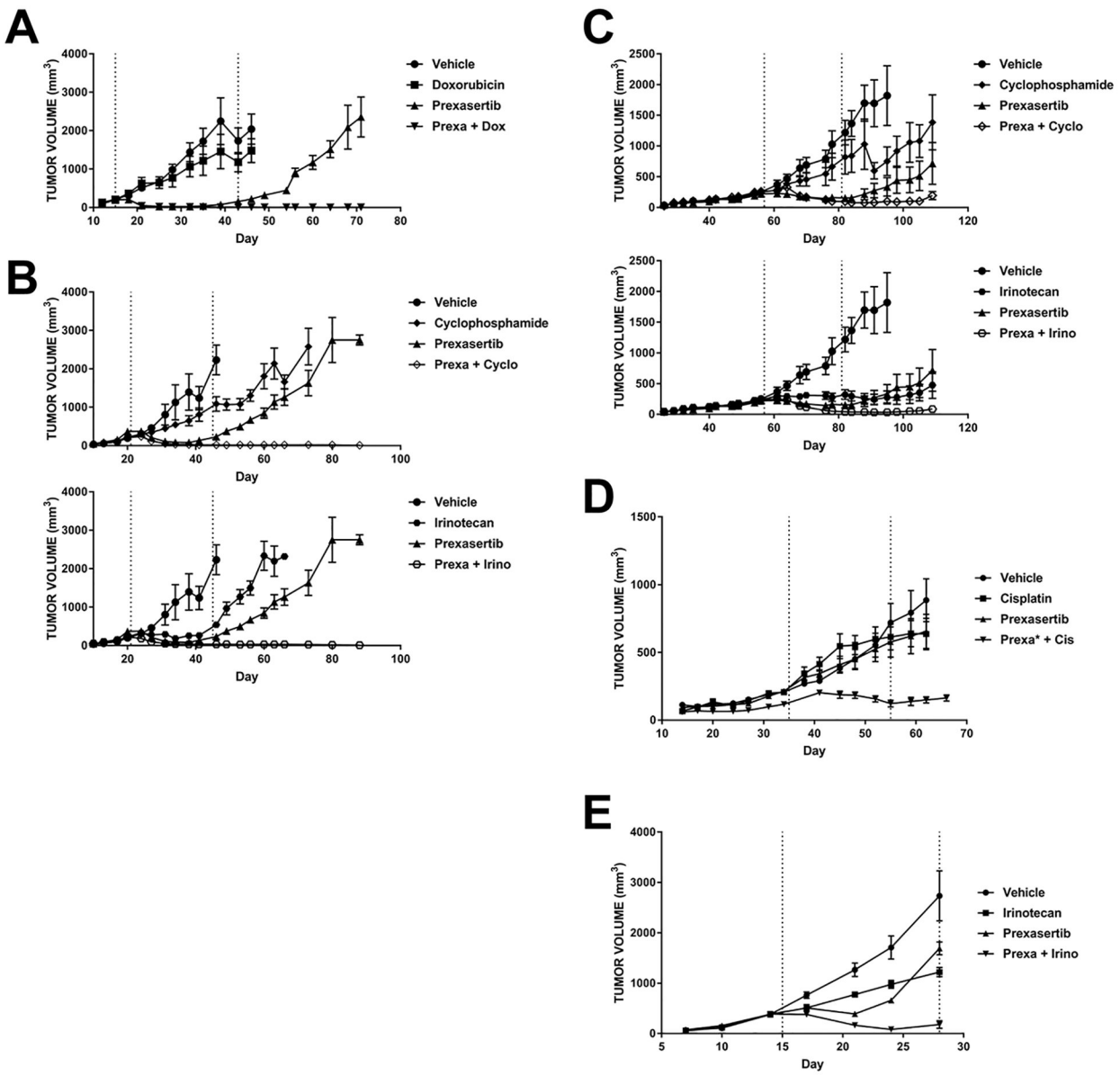

Figure 5. Concurrent administration of chemotherapy prevents acquired resistance and overcomes intrinsic resistance to prexasertib monotherapy.

Animals bearing xenografts of pediatric bone or soft tissue sarcoma were treated with vehicle, prexasertib, chemotherapy, or the combination of prexasertib plus chemotherapy. The specific chemotherapy used is indicated in the key in each panel. **A** and **B**, SJCRH30 alveolar RMS CDX, n = 5/arm for each experiment. **C**, Rh41 alveolar RMS CDX, n = 4/arm. **D**, CCSARC005 osteosarcoma PDX, n = 5/arm, prexa* = dose reduced from 10 mg/kg to 8 mg/kg only in the combination due to use of SCID animals (this model only). **E**, A673 Ewing's sarcoma CDX, n = 5/arm. For **B** and **C**, single experiments are displayed in two different graphs with the same vehicle and prexasertib arms but different chemotherapy and combination arms for clearer visualization. Dotted vertical lines: dosing interval; error bars:

SEM. Waterfall plots for each model are displayed in Supplementary Fig. S4 and statistical analyses are summarized in Supplementary Table S3.

Table 1.

Relative EC50 values of prexasertib in a panel of pediatric cancer cell lines.

Cell Line	Histology	p53 status[^]	EC_{50} (nM)	Max. inhibition[†]
Karpas-299	anaplastic large-cell lymphoma	mutant	0.9	100 ± 0.01
COG-LL-317	acute lymphoblastic leukemia	wild type	2.6	100 ± 0.01
CCRF-CEM	acute lymphoblastic leukemia	mutant	3.0	100 ± 0.00
MOLT-4	acute lymphoblastic leukemia	wild type	3.4	100 ± 0.01
RS4;11	acute lymphoblastic leukemia	wild type	4.5	100 ± 0.00
NALM-6	acute lymphoblastic leukemia	wild type	5.1	100 ± 0.00
Kasumi-1	acute myeloid leukemia	mutant	3.5	97.6 ± 0.10
SJCRH30	alveolar rhabdomyosarcoma	mutant	1.4	99.3 ± 0.04
SJCRH30[*]	alveolar rhabdomyosarcoma	mutant	2.9	96.8 ± 0.37
Rh41	alveolar rhabdomyosarcoma	mutant	8.8	96.6 ± 0.51
Rh41[*]	alveolar rhabdomyosarcoma	mutant	5.5	92.2 ± 1.22
RD	embryonal rhabdomyosarcoma	mutant	22	87.0 ± 0.57
RD[*]	embryonal rhabdomyosarcoma	mutant	9.1	74.0 ± 2.27
Rh18	embryonal rhabdomyosarcoma	wild type	2.9	88.6 ± 1.70
A673[*]	Ewing's sarcoma	mutant[≠]	5.2	75.9 ± 2.80
CHLA-9	Ewing's sarcoma	wild type	1.6	98.7 ± 0.20
TC-71	Ewing's sarcoma	mutant[≠]	1.6	100 ± 0.00
CHLA-10	Ewing's sarcoma	mutant	1.7	99.3 ± 0.20
CHLA-258	Ewing's sarcoma	wild type	2.4	89.8 ± 0.30
SJ-GBM2	glioblastoma	mutant	2.6	98.5 ± 0.13
BT-12	atypical teratoid/rhabdoid tumor	wild type	6.6	80.2 ± 0.70
CHLA-266	malignant rhabdoid tumor	wild type	15	55.5 ± 1.69
CHLA-136	neuroblastoma	wild type	0.9	87.2 ± 1.02
NB-EBc1	neuroblastoma	wild type	1.7	98.7 ± 0.12
CHLA-90	neuroblastoma	mutant	3.7	91.9 ± 0.19
NB-1643	neuroblastoma	wild type	4.8	97.6 ± 0.07
Ramos-RA1	non-Hodgkin's lymphoma	mutant	6.5	99.5 ± 0.01
MG-63[*]	osteosarcoma	mutant[≠]	8.1	97.7 ± 0.18

[*] calculated from 72h timepoint

[^] p53 status previously reported in Carol H et al. Initial testing of the MDM2 inhibitor RG7112 by the Pediatric Preclinical Testing Program. Pediatr Blood Cancer 2013;60(4):633–41.

[≠] p53 status previously reported in Ottaviano L et al. Molecular characterization of commonly used cell lines for bone tumor research: a trans-European EuroBoNet effort. Genes Chromosomes Cancer 2010;49(1):40–51.

[†] Inhibition achieved at 1 μM prexasertib, calculated as (1-(treated/control)*100%) and reported as %Max Inhibition ± SEM; complete curves shown in Supplementary Fig. S1.